1986A&A...167..351T

Astron. Astrophys. 167, 351–358 (1986)

ASTRONOMY AND ASTROPHYSICS

Emission of Lyman-α radiation by solar coronal loops

II. Filtergram analysis

G. Tsiropoula [1], C. Alissandrakis [2], R.M. Bonnet [3], and P. Gouttebroze [4]

[1] National Observatory of Athens, Astronomical Institute, GR-11810 Athens, Greece
[2] Section of Astrophysics, Astronomy and Mechanics, Department of Physics, University of Athens, GR-15771 Athens, Greece
[3] European Space Agency, 8–10, rue Mario Nikis, F-75738 Paris Cedex 15, France
[4] Laboratoire de Physique Stellaire et Planétaire, B.P. n^0 10, F-91371 Verrières le Buisson Cedex, France

Received March 11, accepted June 2, 1986

Summary. We study active region loops, observed on Lα high resolution filtergrams obtained with a rocket borne instrument. Some formulae or diagrams are given for the computation of Lα and Hα intensities emitted by homogeneous loop models. The dimensions and emitted intensities of the observed loops being known, we determine the variations of temperature, pressure and density inside these objects under the assumption of constant temperature and hydrostatic equilibrium. The influence of temperature gradient and mass flow on our results is discussed, and an alternative model with radial temperature increase is envisaged. The case of an isolated loop with a larger diameter is also discussed.

Key words: Sun – corona – Lyman-α – loops

1. Introduction

In recent years much effort has been directed towards the study of the physical and dynamical structure of the solar corona. The most significant contribution has, undoubtedly, come from the high-resolution observations made from space at UV, EUV, XUV, and X-ray wavelengths by instruments on board OSO satellites, Skylab and recently SMM. These observations have confirmed the complex loop-like structuring of the outer solar atmosphere and established the dominant role of the magnetic field in the geometric arrangement of the coronal plasma. The loop-like structures have various sizes, densities, temperatures and lifetimes (Withbroe and Noyes, 1977) and occupy a significant fraction of the solar chromosphere and corona. Therefore, their dynamical and thermal properties are fundamental in enlarging our understanding of coronal heating and energy balance.

Since loops are the basic "building block" of the outer layers of the solar atmosphere, it is important to determine observationally their physical individual properties; this is an essential first step towards the construction of realistic models of active regions and also towards the understanding of the physics and dynamics of the solar corona.

The aim of this paper is to present the diagnostic possibilities resulting from the theoretical study of the emission of Lα radiation by coronal structures (Gouttebroze et al., 1986, hereafter referred to as Paper I), in the analysis of Lα filtergrams such as those obtained with the "Transition Region Camera" (TRC) (Bonnet et al., 1980), and, especially, in the determination of physical properties of loop structures observed at the limb.

Send offprint requests to: G. Tsiropoula

2. Computation of Lyman-α Intensities

2.1. Principal results from Paper I

The formation of Lyman-α in loops was investigated, both in the optically thin and thick cases. In particular, we obtained the intensity emitted by a loop seen at the solar limb, as a function of its pressure, temperature and geometrical thickness.

In the optically thin case, both optical thickness and emitted intensities decrease regularly with temperature. It is possible to obtain approximate empirical relations to describe the variations of these quantities. Applying a least-square method to the results of Paper I, we obtain, for the optical thickness at line center:

$$\tau_0 = P\,\Delta l\,10^{a_0 + a_1 x + a_2 x^2 + a_3 x^3} \quad (1)$$

with $a_0 = -0.028$, $a_1 = -3.840$, $a_2 = 0.703$ and $a_3 = -0.183$. P is the pressure in dyn cm^{-2}, Δl the geometrical thickness in Mm and x is a function of the temperature: $x = \log(T/10^5\,\mathrm{K})$.

For the neutral hydrogen density, we obtain a similar relation:

$$N_1 = P\,10^{b_0 + b_1 x + b_2 x^2 + b_3 x^3} \quad (2)$$

with $b_0 = 5.748$, $b_1 = -3.381$, $b_2 = 0.712$ and $b_3 = -0.183$.

As in Paper I, we use a relative intensity scale, defining the "Lyman-α relative intensity" (LRI) as the intensity in a 10 nm bandpass around the line divided by the same quantity averaged on the solar disk. For the optically thin case, we obtained in Paper I the following formula:

$$\mathrm{LRI} \simeq \Delta l\left[1.3\ 10^{-4}\left(\frac{T}{10^6}\right)^{-3} P + 2.1\ 10^{-4}\left(\frac{T}{10^6}\right)^{-3.5} P^2\right]. \quad (3)$$

In the optically thick case, the variation of intensity with temperature is more complicated (nonmonotonic) and the intensity is no more proportional to the thickness. Then, it is

© European Southern Observatory • Provided by the NASA Astrophysics Data System

1986A&A...167..351T

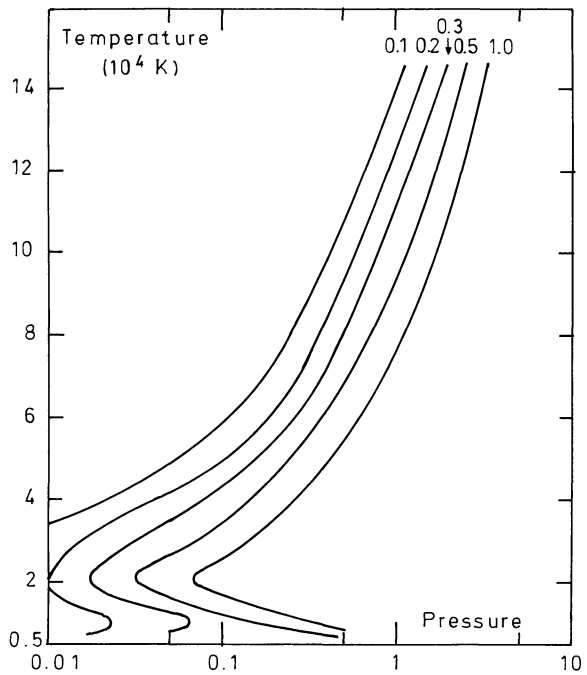

Fig. 1. Temperature as a function of pressure (in dyn cm^{-2}) for an object of thickness 1 Mm observed at the solar limb. Each curve corresponds to a constant value of LRI (indicated at the top)

necessary to use point-by-point computed diagrams such as that represented in Fig. 7 of Paper I.

Using these formulae and diagrams, it is possible, once the diameter of an homogeneous loop and the emitted intensity are known, to deduce a relation between its pressure and temperature. Such relations are represented in Fig. 1 for a loop diameter of 1 Mm and different values of the LRI.

2.2. Additional results

A new set of computations, similar to that of Paper I, has been done to determine the intensities emitted by vertical slabs at the solar limb. The thickness chosen, 2 Mm, corresponds to the diameter of observed loops studied in Sect. 4. The values of pressure and temperature investigated correspond to LRI in the range [0.02, 1], since structures brighter than the solar disk were not observed at the limb and, on the other hand, objects with LRI lower than 0.02 are completely invisible on the filtergrams. In order to obtain reliable Hα intensities, we used a 5 level plus continuum hydrogen atom. Frequency redistribution was assumed to be partial in Lα and Lβ, and complete in other lines. Other details on these computations are given in Paper I.

The variation of emitted intensities in Lα, as a function of pressure and temperature, is represented in Fig. 2a. At low pressures ($P \leqq 0.1$ dyn cm^{-2}) and temperature ($T \leqq 10000$ K), the curves are nearly flat, so that the relative intensity may be a good indicator of pressure. One may see also that, for temperatures lower than 20000 K, it is practically impossible to obtain a LRI lower than 0.1, unless assuming pressures lower than 10^{-3} dyn cm^{-2}, because the objects remain optically thick. It is a strong argument to suggest that an observed LRI of, e.g., 0.05 corresponds to an optically thin object located on the high temperature side of the diagram.

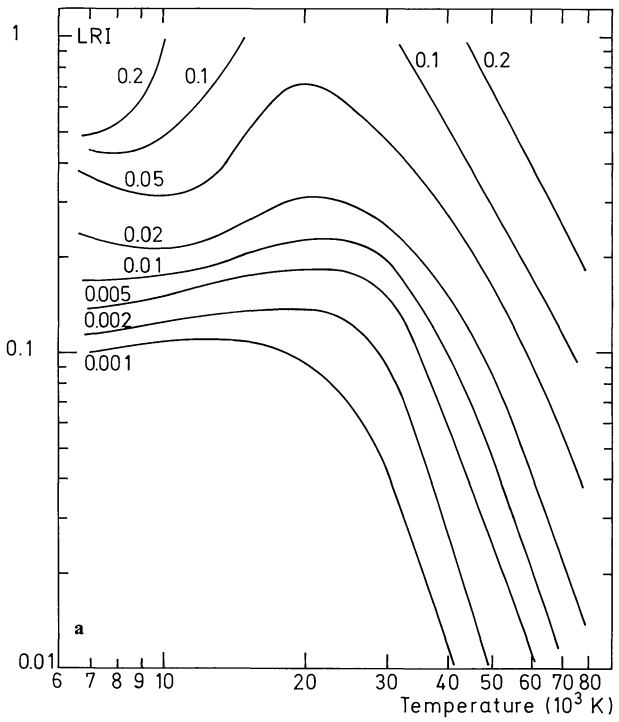

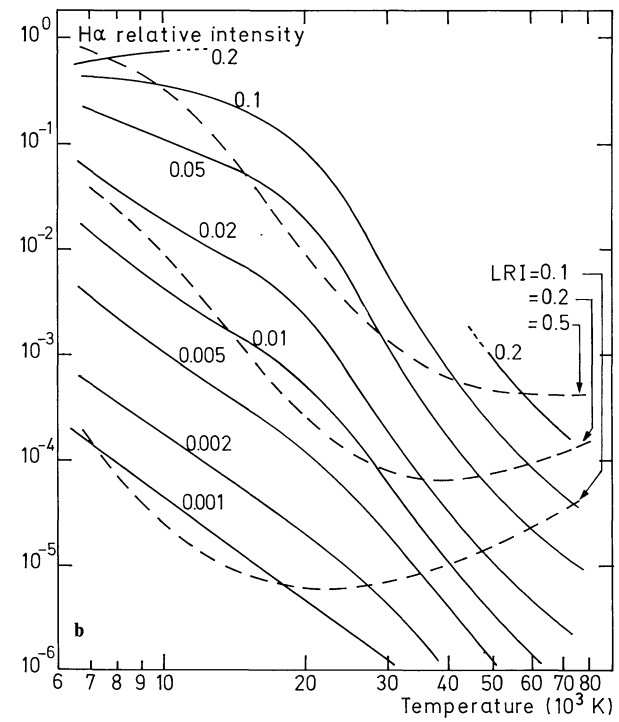

Fig. 2. **a** Variation of Lyman-α relative intensity, as a function of pressure and temperature, for a slab of thickness 2 Mm at the solar limb, standing perpendicularly to the line of sight of the observer (each curve corresponds to a given pressure indicated, in dyn cm^{-2}, along the curves). **b** Same curves for the relative intensity at the center of the Hα line. The dashed lines correspond to constant-LRI curves (0.1, 0.2, and 0.5)

© European Southern Observatory • Provided by the NASA Astrophysics Data System

1986A&A...167..351T

2.3. Intensities in Hα

Figure 2b represents the corresponding intensities at the center of the Hα line, relative to the mean intensity of the solar disk at the same frequency. In the ranges of pressure and temperature considered, most objects are optically thin in Hα, and the curves show a regular decrease of intensity with temperature, due to that of optical thickness.

If simultaneous observations of Hα and Lα are available, the use of these two diagrams may in principle allow a diagnostic of the physical conditions in the loops. For instance, we consider a loop with a diameter of 2 Mm and a LRI of 0.2 along its axis. Using Fig. 2a, we determine the possible values of pressure and temperature: for $P \leqq 0.005$ dyn cm^{-2}, there is no solution; for $P = 0.01$, two different temperatures are possible, 14000 K on the cool (optically thick) side and 29000 K on the hot (optically thin) side; for higher pressures, there is only one possible temperature, on the hot side of the curves. Then, using Fig. 2b, it is possible to determine the corresponding Hα intensities and to draw approximate Lyman-isophotes on the Hα intensity diagram. Such isophotes, corresponding to LRI of 0.1, 0.2 and 0.5 are represented in Fig. 2b. For LRI = 0.5, the Hα relative intensity of the object may vary by more than 3 orders of magnitude, according to its temperature. If the limit of detectability on Hα spectroheliograms is, e.g., 0.01, a loop with LRI = 0.5 will be visible in Hα if its temperature is lower than 20000 K and invisible otherwise. Loops with LRI = 0.2 will appear on Hα spectroheliograms only if they are very cold (less than 10000 K), while those with LRI = 0.1 should normally never appear on these pictures. In brief, one may conclude that objects clearly visible at the solar limb both in Hα and Lα are cool, while those which are bright in Lα and invisible in Hα are relatively hot.

3. Observations

3.1. Description

High resolution (~1″) Lα pictures of the Sun have been obtained during the flight of a Black Brant rocket which took place on July 3rd, 1979, with a rocket borne telescope. The experiment was conducted jointly by the Lockheed Palo Alto Research Laboratory and the Laboratoire de Physique Stellaire et Planétaire du CNRS and investigated the transition region plasma and the geometry of coronal active regions.

The solar images were recorded on Kodak 101–01 film. A series of five exposure times was programmed and commanded through an electronic sequencer: 0.06 s, 0.125 s, 0.23 s, 0.325 s, and 1.0 s in order to have both the brightest active regions and the faintest features at the limb (for more details, see Bonnet et al., 1980).

These L α pictures clearly showed intermingling chromospheric and coronal structures whose shapes and orientations were likely governed by the magnetic field. Especially, they revealed complex loop-like structures connecting the various parts of active regions; these loops can be seen either in emission at the limb and in emission or in absorption over the solar disk. Such structures are probably similar to the cold loops seen in emission in the EUV even at altitudes as high as 10^5 km (Foukal, 1976).

3.2. Data reduction and calibration

We made microdensitometer raster scans of two Lα photographic images, which had different exposure times. On the 0.325 s photographic image the entire solar disk having a 23.1 mm diameter was scanned. The step size in both horizontal and vertical directions was 20 μm. On the more exposed 1 s photographic image, structures seen at the limb were scanned with a step size of 10 μm, which corresponds to about 600 km on the Sun. The raster scans result in two-dimensional maps of optical density. Two pieces of Kodak 101–01 film were used for the photometric calibration; they were exposed to the light of a standard source with the same illumination and different exposure times, because of the very good response of this film to the reciprocity law: one of the these films was placed in a container and flew with the instrument, while both were developped in the same processing run after the flight.

The precise determination of LRI in loops required the use of two different pictures with different exposure times, since the center of the solar disk was overexposed on 1 second pictures, while the loops were underexposed on other ones. As the slopes of the calibration curves were the same for the different exposure times, we used the following procedure: using a picture with 0.325 s exposure time, we determined the mean intensity I_D near the center of the disk, relatively to an area with a given optical density (say, $D = 1$). We performed the same operation to obtain relative loop intensities I_L on the picture with 1 s exposure time. Finally, we deduced the loop intensity relative to the mean disk center: LRI $= 0.325\, I_L/I_D$. The validity of this method was checked on several areas of intermediate intensity visible on both pictures.

3.3. A group of active region loops

Some physical properties of the loops observed on the Lα filtergrams obtained with TRC can be obtained from the photometric analysis. On the more exposed film we selected two loops lying over the active region McMath 16123, very close to the Eastern limb, hereafter called loop 1 and loop 2 (Fig. 3a), for which only one leg was observed. This choise was made because these loops could be identified easily and singled out from their neighbors. Using the characteristic curve we converted the optical density maps to relative intensity maps. On Figure 3b, we represent the variations of LRI perpendicularly to the axis of the loops 1 and 2 at different positions. Position 1 (Fig. 3b) corresponds to an arbitrary base above the limb, where the film density is in the linear part of the characteristic curve. The distance between two successive positions corresponds to ~750 km on the Sun. These profiles of transverse intensity variation were corrected by subtraction of a residual emission from neighbor loop structures, the background emission and the stray light. From every corrected profile we measured the LRI on the loop axis. In Figs. 4a and b we plot the LRI as a function of the distance from the base of the loops. The error in the LRI determination is of the order of ± 0.01 and is due to the noise from the film grains. From Figs. 4a and b we can see that above the chromospheric limb there is an increase of LRI for both loops. Subsequently the LRI of loop 1 decreases to undetectable levels, while that of loop 2 remains constant for some distance and after that decreases also to undetectable levels. Both loops show intensity fluctuations which are not much larger than our estimated error.

From every corrected profile (of transverse intensity variation) also measured the full width at the half maximum. The values of the diameter thus obtained are shown in Fig. 5a and b as a function of position along the loops and were determined to an accuracy of about ± 0.12 Mm. Within the errors of the measurement the diameter shows a remarkable constancy.

© European Southern Observatory • Provided by the NASA Astrophysics Data System

1986A&A...167..351T

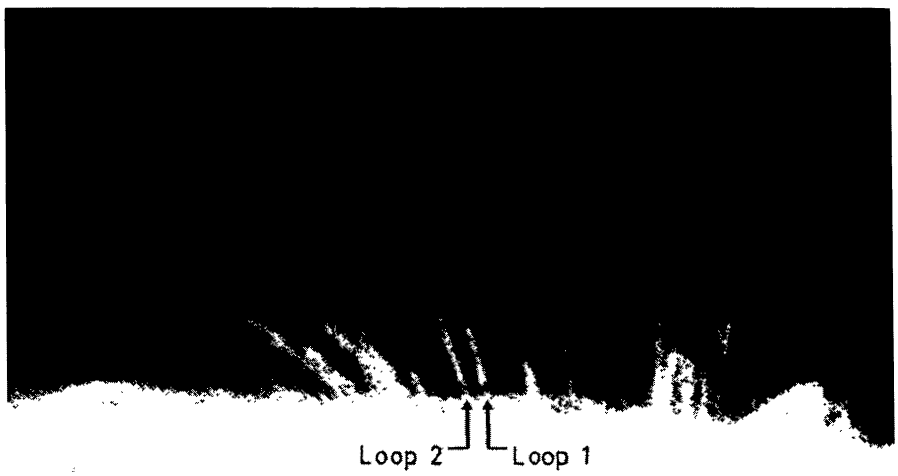

Fig. 3a

Fig. 3. **a** A loop system associated with an active region, observed at the limb by the TRC in the Lα line. Loops 1 and 2 used in this study are shown. **b** Isophote map of loops 1 and 2. The length of the bars is equal to 2 Mm in both horizontal and vertical directions. The limb is also shown

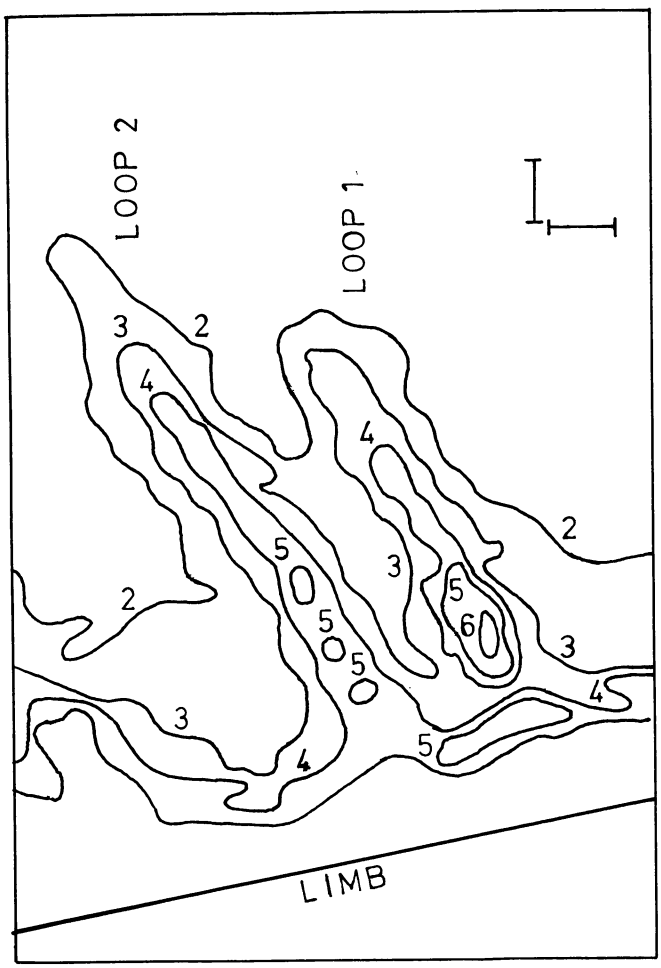

Fig. 3b.

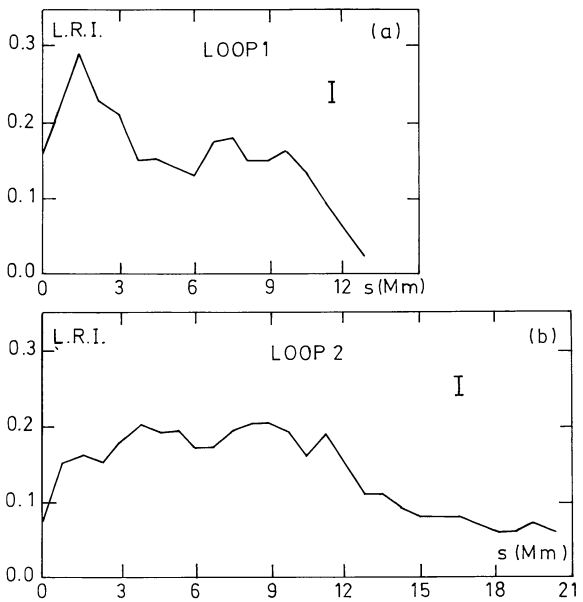

Fig. 4a and b. Variation of Lα relative intensity (LRI) along the axes of loops 1 and 2. The error of the determination is of the order of 0.01

4. Analysis of two active region loops

4.1. Determination of a relation between pressure and temperature

There is a wide range of different types of loops. In Priest's (1978) classification, active region loops vary in length from 10 Mm to 100 Mm, have densities from 5 to 50 10^{14} cm^{-3} and temperatures from 10^4 to 2.5 10^6 K. In this section we shall try to determine the physical conditions in the two active region loops described in 3.3.

© European Southern Observatory • Provided by the NASA Astrophysics Data System

1986A&A...167..351T

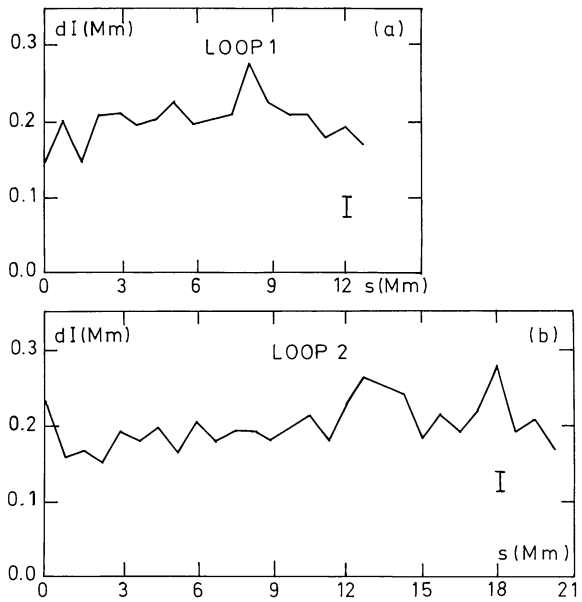

Fig. 5a and b. Variation of diameters along the axes of loops 1 and 2. The error of the determination is of the order of 0.12 Mm

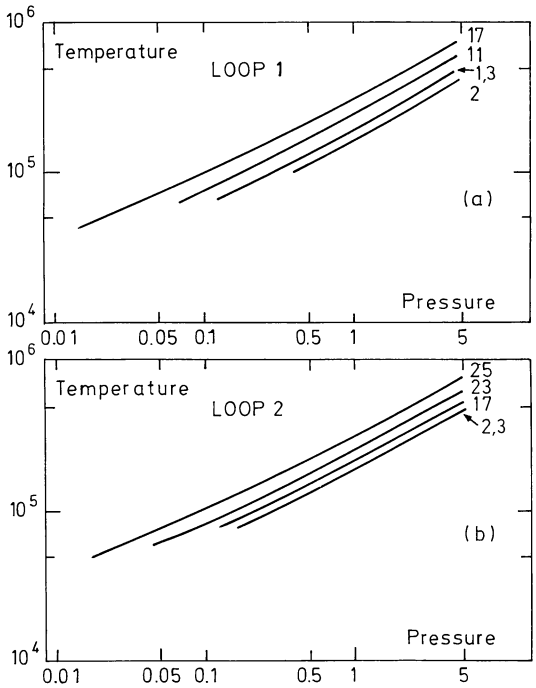

Fig. 6a and b. Possible values of temperature as a function of pressure at some positions of loops 1 and 2; these positions are indicated at the right top of each curve (only the parts of the curves for which $\tau_0 \leqq 1$ are represented)

However, the precise knowledge of the physical conditions within these structures is impossible without further assumptions, because we have to determine at least two unknowns (temperature and pressure) from only one piece of information (intensity). With our data and no further assumptions we can only give a relation between the temperature and the pressure at the different positions of the loops. These loops are invisible on any available Hα spectroheliogram taken during the same day (July 3, 1979) while, for instance, the prominence located on the Eastern limb near the North Pole (latitude $\sim 72°$) is clearly visible both on Hα and Lα pictures. This suggests, from computations of Sect. 3, that these loops are not very cold objects ($T \leqq 15\,000$ K) and that they should be located on the "optically thin" side of the diagram of Fig. 2a. In this case, the empirical relation (3) remains roughly valid. Using this relation, we can determine, once the LRI and the diameter of the loop are known, a pressure-temperature relation. This has been done for the loops 1 and 2 and for a reasonable range of pressures: $0.01\ \mathrm{dyn\,cm^{-2}} \leqq P \leqq 5\ \mathrm{dyn\,cm^{-2}}$. These relations are represented in Fig. 6 for different positions along the two loops.

4.2. Determination of the loop temperature and pressure under isothermal assumption without mass flow

In order to get definite values for the temperature and pressure we need additional information. Until now comprehensive models of loops do not exist, since such models should take into account magnetic fields, gravity, geometry, radiation losses, heating, thermal conduction, mass flow, etc. The procedure usually followed, in order to make the problem easier, is to neglect some of the terms that enter the MHD equations. The efforts towards the construction of loop models, so far presented, fall in two different groups. One is the costruction of static models based on energy balance arguments, without mass flows (Rosner et al., 1978; Hood and Priest, 1979; Serio et al., 1981). The other group is that of dynamical models with mass flows ($\boldsymbol{u} \neq 0$). These models have received much less attention (see however Cargill and Priest, 1980; Noci, 1981 and a review by Priest, 1981, where the general effects of dynamics in active regions are described).

To solve the problem of the indetermination mentioned above, we make some physical assumptions resulting in a very simplified model. We assume that the flow speed is much lower than the sound speed (which is of the order of $\sim 40\ \mathrm{km\,s^{-1}}$ for a temperature $T \sim 1\ 10^5$ K) and so we can neglect flows. We also assume that the temperature is constant along a loop. Except at the lowest boundaries, i.e. the legs of a loop, where the temperature may drop rapidly to that of the chromosphere, this is a reasonable assumption due the high thermal conductivity along the magnetic field.

For a constant temperature loop with negligible flow, the pressure distribution is given by the equation of hydrostatic equilibrium:

$$P(h) = P_0 \exp(-h/H), \tag{4}$$

where P_0 is the pressure at the base of the loop, h the altitude and H the pressure scale height ($H \simeq 5\ 10^3\ T$ cm).

Thus, our hydrostatic and isothermal model is defined by two parameters: the base pressure P_0 and the temperature T. The values of these parameters are determined iteratively: starting from an arbitrary value of temperature, we calculate the pressure at any position along the loop using relation (3) and the known values of LRI and diameter. Then from the variation of pressure with height we compute the mean scale height using Eq. (4) and hence a new value of the temperature. The procedure is repeated until self consistent results are obtained. The method converges very rapidly because the successive curves of the pressure vs height are almost parallel.

In Figs. 7a and b, we show the variation of the natural logarithm of pressure as a function of height above the limb for the final values of temperature found as previously described. Loop 1 shows a reasonable agreement with the model, while for loop 2 this

© European Southern Observatory • Provided by the NASA Astrophysics Data System

1986A&A...167..351T

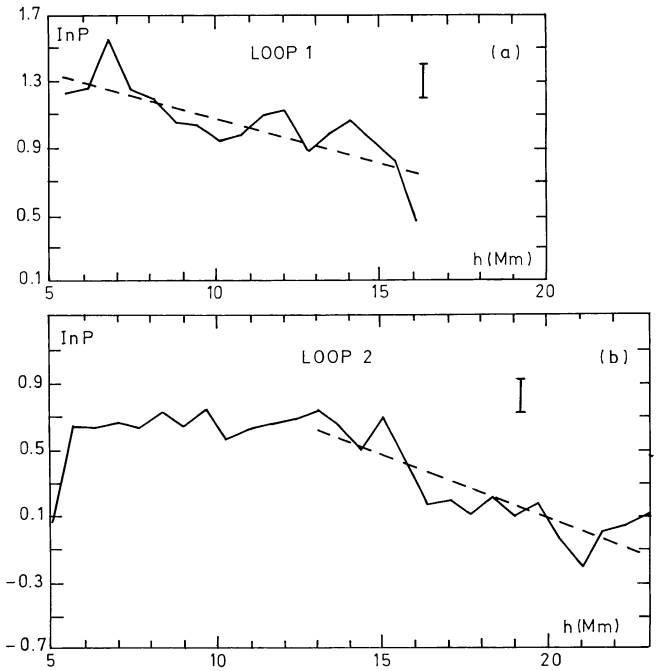

Fig. 7a and b. Variation of the logarithm of pressure as a function of the height from the limb for loops 1 and 2. The dashed lines give the best fit to an isothermal model without mass flow

is true only for heights above 13 Mm. The values of the temperature are $(3.6 \pm 0.7)\ 10^5$ K and $(2.6 \pm 0.4)\ 10^5$ K for 1 and 2 respectively, while those of base pressure are (5.2 ± 0.6) dyn cm^{-2} and (4.9 ± 1.1) dyn cm^{-2}.

Using the empirical relation (1) for optical depths, as well as the empirical relation (2) for neutral hydrogen densities we obtain the variations of these parameters along the two loops. So for loop 1, the transverse optical thickness varies from 0.08 to 0.03 and neutral hydrogen densities from 5.4 10^4 to 1.8 10^4 cm^{-3}, while the corresponding values for loop 2 are in the range (0.11, 0.05) and (5.5 10^4, 2.2 10^4) cm^{-3}.

4.3. Influence of temperature gradient and mass flow

Recent observations have stressed that active region loops can be divided into loops having temperatures greater than 10^6 K and loops where ions formed at transition region temperatures are observed. Foukal (1975, 1976, 1978) analyzing loops of this category, found that they extend upto altitudes much beyond their scale height, in contradiction with hydrostatic equilibrium. Raymond and Foukal (1982) and Doyle (1985) found that the physical parameters derived from the UV spectra cannot be reconciled with the scaling laws derived from static loop models. This is attributed to the presence of downflows. In fact, nonthermal velocities in the range of 30–100 km s^{-1} have been inferred from Doppler shift measurements in lines of Si IV, C IV and other transition ions (Bruner et al., 1976; Doschek et al., 1976) in areas such as spots, plages and network where coronal loops are likely to be rooted. Therefore a more complete model must consider the case of $u \neq 0$ and also a possible existence of temperature gradients.

We examine below the consequences of relaxing our preceding assumptions on the loop model.

4.3.1. Temperature constant – $u \neq 0$

Mass flow will decrease the pressure below the hydrostatic equilibrium value; this decrease is more important for high values of the flow velocity. Then, if the velocity increases with heigth as is the case in subsonic flows (Cargill and Priest, 1980), the pressure gradient will be larger and the scale height smaller than in the stationary case. Consequently, the temperature determined by our method will be a lower limit.

4.3.2. Longitudinal temperature gradient

Although strong temperature gradients parallel to the magntic field lines are unlikely, Levine and Withbroe (1977) reported a significant temperature gradient along the field lines of an active region loop, the temperature maximum being located near the top, and concluded that there is local energy deposition within the loop.

Such a positive temperature gradient would result in a faster decrease of Lyman-α intensity with altitude, according to Eq. (3). Therefore, if hydrostatic equilibrium is maintained, it would be necessary to increase the pressure scale height, i.e. the temperature, to obtain the same intensity variation. Conversely, the introduction of a negative temperature gradient would result in a decrease of the mean temperature of the model.

4.3.3. Radial temperature gradient

Multi-line observations made with the Harvard spectrometer on Skylab have shown the existence of active region loops with temperature increasing radially from the axis to the external corona (cf. Foukal, 1975, 1976; Levine and Withbroe, 1977). In this case, the difficulty of a diagnostic lies in the fact that the cool cores of the loops, if they exist, are not resolved.

For instance, Levine and Withbroe propose a loop core with a radius of 133 km in the C II line (about 45000 K). As the spatial resolution of TRC is limited to about 700 km (Bonnet et al., 1980), a possible optically thick cool core (i.e. with a LRI of order 0.5) would be spread by the instrumental function and could not be distinguished from the surrounding, optically thin, regions. All that we can say is that the diameter of the cool core, if it exists, is certainly smaller than the measured diameter of the loop, i.e. 2000 km (the upper limit deduced from Skylab observations was 3500 km). The fact that these loop cores were not detected on the Hα spectroheliograms is not significant, because their expected dimensions are small with respect to the angular resolution of these pictures.

5. A closed, isolated loop

Among different objects that can be seen at the solar limb on Lyman-α filtergrams, there is a conspicuous loop, with regular shape, represented in Fig. 8a. This loop, which appears on the Western limb near the equator, is very likely rooted in a small plage of the active region McMath 16100. Figure 8b represents the isophote map of this loop in Lα. This loop has an approximately constant diameter of (3.5 ± 0.5) Mm. The LRI is about 0.5 at the top and 0.2 in the feet. This loop is undetectable on Hα spectroheliograms taken during the same day.

Contrary to the active region loops described in the preceding sections, where the LRI was decreasing regularly with altitude, the present loop is brighter at the top than in the feet. Thus, the isothermal-hydrostatic assumption used in the preceding sections

© European Southern Observatory • Provided by the NASA Astrophysics Data System

1986A&A...167..351T

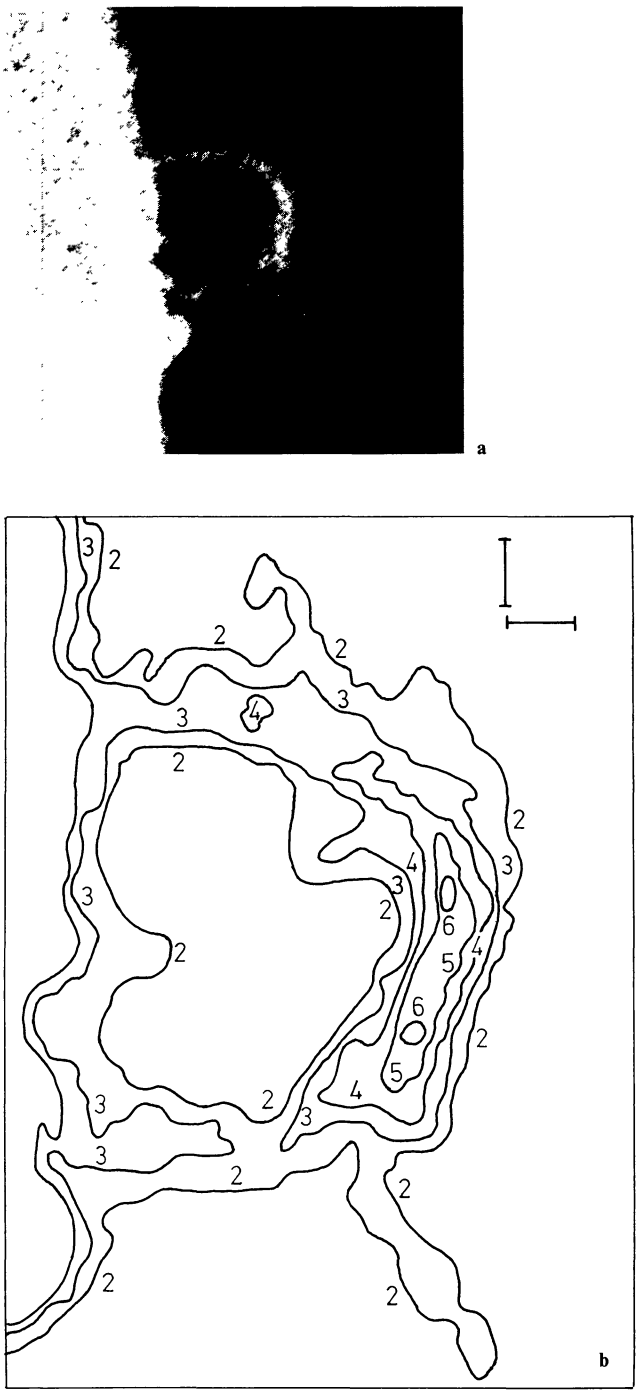

Fig. 8. a An isolated, closed loop at the limb observed in the Lyman-α line with TRC. **b** Isophote map of the same loop. The length of the bars corresponds to 3 Mm

must be ruled out in this case. This reinforcement of intensity at the top of the loop might be explained in different ways. For instance, if the plane of the loop is not perpendicular to the line of sight but makes a small angle with it, the loop will appear thicker (geometrically and optically) at the top than in the feet. But, the general appearance of this object, as seen in Fig. 8a, makes this explanation unlikely. So, we prefer the following one: among theoretical loop models discussed by Serio et al. (1981), there are so-called "class II loops" with a minimum of temperature at the top. As the loop under consideration does not appear on Hα spectroheliograms, we can, using the diagram of Fig. 2b, rule out the very low temperature range (0–15 000 K). At temperatures higher than 20 000 K, the intensity in Lα is a decreasing function of temperature, so that the reinforcement of intensity at the top of the loop is consistent with a "class II" loop structure.

6. Conclusion

The Transition Region Camera has observed a system of active region loops at the solar limb in the Lyman-α line. The apparent diameter of these loops is of order 2 Mm, and the intensity is rapidly decreasing with altitude, so that the top of these loops is not visible. If these objects are in hydrostatic equilibrium and if their temperature is constant, the variation of intensity with altitude implies temperatures in the range $2\ 10^5$ K to $5\ 10^5$ K, and base pressures of order 5 dyn cm^{-2}. The addition of a stationary flow into the loop model would require an increase of the mean temperature. Models with longitudinal temperature gradients should be in average hotter (resp. cooler) than the isothermal one, if the temperature increases (resp. decreases) with height. If (non-equilibrium) models with cool cores and radial temperature increase are valid, the present observations indicates that these cores have a diameter smaller than 2000 km.

Whatever their quality, Lyman-α filtergrams cannot give by themselves unambiguous diagnostics of coronal loops. Nevertheless, observations in this line remain the best means to study the cold components of the solar corona. The usefulness of multi-line observations has been evidenced by the Skylab Harvard experiment. For very cool structures, simultaneous observations in Lα and Hα should be useful. Simultaneous measurements of Lα profiles would be necessary to obtain a reliable determination of temperature. Finally, the question of the existence of very cool loop cores would require, to be definitively answered, a very important improvement of angular resolution, which is unfortunately improbable in the near future.

Acknowledgements. We thank Mrs Martres (DASOP, Meudon Observatory), for providing us with Hα spectroheliograms, and J.C. Vial for critical reading of the manuscript.

Numerical calculations of Sect. 2 used computer time allocated by the Scientific Comittee of "Centre de Calcul Vectoriel pour la Recherche" (Palaiseau, France).

References

Bonnet, R.M., Bruner, E.C. Jr., Acton, L.W., Brown, W.A., Decaudin, M.: 1980, *Astrophys. J.* **237**, L47

Bruner, E.C., Chipman, E.G., Lites, B.W., Rottman, G.J., Shine, R.A., Athay, R.G., White, O.R.: 1976, *Astrophys. J. Letters* **210**, L97

Cargill, P.J., Priest, E.R.: 1980, *Solar Phys.* **65**, 251

Doschek, G.A., Feldman, V., Bohlin, J.D.: 1976, *Astrophys. J. Letters* **205**, L177

Doyle, J.G., Mason, H.E., Vernazza, J.E.: 1985, *Astron. Astrophys.* **150**, 69

© European Southern Observatory • Provided by the NASA Astrophysics Data System

1986A&A...167..351T

Foukal, P.V.: 1975, *Solar Phys.* **43**, 327
Foukal, P.V.: 1976, *Astrophys. J.* **210**, 575
Foukal, P.V.: 1978, *Astrophys. J.* **223**, 1046
Gouttebroze, P., Vial, J.C., Tsiropoula, G.: 1986, *Astron. Astrophys.* **154**, 154 (Paper I)
Hood, A.W., Priest, E.R.: 1979, *Astron. Astrophys.* **77**, 233
Levine, R.H., Withbroe, G.L.: 1977, *Solar Phys.* **51**, 83
Noci, G.: 1981, *Solar Phys.* **69**, 63
Priest, E.R.: 1978, *Solar Phys.* **58**, 57
Priest, E.R.: 1981, in *Solar Active Regions*, ed. F. Orrall, Univ. of Colorado ASS. Press
Raymond, J.C., Foukal, P.V.: 1982, *Astrophys. J.* **253**, 323
Rosner, R., Tucker, W.H., Vaiana, G.S.: 1978, *Astrophys. J.* **220**, 643
Serio, S., Peres, G., Vaiana, G.S., Golub, L., Rosner, J.: 1981, *Astrophys. J.* **243**, 288
Withbroe, G.L., Noyes, R.W.: 1977, *Ann. Rev. Astron. Astrophys.* **15**, 363

© European Southern Observatory • Provided by the NASA Astrophysics Data System